Desalination and Water Treatment
www.deswater.com
doi: 10.1080/19443994.2015.1085451

57 (2016) 17151–17166
August

Taylor & Francis
Taylor & Francis Group

Experimental and theoretical performance of finned-single effect solar still

M. El-Naggar*, A.A. El-Sebaii, M.R.I. Ramadan, S. Aboul-Enein

Faculty of Science, Department of Physics, Tanta University, Tanta, Egypt, Tel. +20 0403344352; Fax: +20 0403350804; emails: mohammed_elnaggar2020@yahoo.com, mohammedelnaggar.science.tanta.edu.eg (M. El-Naggar), ahmedelsebaii@yahoo.com, ahmed.elsebaei@science.tanta.edu.eg (A.A. El-Sebaii), mohamed.ramadan@science.tanta.edu.eg (M.R.I. Ramadan), saad.aboulenain@science.tanta.edu.eg (S. Aboul-Enein)

Received 29 January 2015; Accepted 15 August 2015

ABSTRACT

A conventional single basin solar still and modified unit with finned-basin liner were constructed and investigated experimentally and theoretically. The stills were tested outdoors on typical days of June 2014 under Tanta prevailing weather conditions (Lat. 30˚ 47′ N, Egypt). The energy balance equations of the considered stills were formulated and solved analytically. Suitable computer programs were prepared for optimizing and predicating the thermal performance of the considered systems. Comparisons between experimental and theoretical results were performed. Comparisons of the obtained results with those presented in previous studies were also made. The daily productivities of the conventional and modified stills were found to be 4.235 and 4.802 (kg/m^2 d) with daily efficiencies of 42.36 and 55.37%, respectively. The convective heat transfer coefficient from the finned plate was increased by 3.6 times compared to the case without fins. The agreement between measured and calculated daily productivity is fairly good. The cost of 1 L of distillate water was found to be 0.28 LE.

Keywords: Desalination; Solar still; Thermal performance; Mathematical model; Fins

1. Introduction

Water is essential for all life forms on the earth, plants, animals, human, etc. The demand of the fresh water is increasing due to population growth and rapid industrialization. Ocean is the only available source for large amount of water. But the ocean water contains high salinity, so it needs to desaline the water. Desalination methods use large amount of energy (fossil fuels) to remove a portion of pure water from a salt-water source. A solar still is a device, which is widely used in solar desalination process to produce potable water from brackish and saline water using solar energy [1].

Solar stills were widely used in solar desalination. The productivity of single effect solar stills is relatively low. To augment the productivity of the single effect solar stills, researchers from all over the world had tested a number of designs and modifications. The various factors affecting the still productivity such as glass cover slope, base insulation, basin water depth, and dye, besides the climatic factors such as solar radiation, wind velocity, ambient temperature, and many other operating factors were investigated. Mathematical modeling, theoretical analysis, and computer simulation of different designs of solar stills had

*Corresponding author.

been presented in a number of articles [2–29]. Many researchers had investigated the effect of solar radiation on productivity, and their results indicated that the still productivity increases with increasing incident solar radiation [2]. A very simple method for increasing the absorption of the basin water is to add dye to the basin water. Results showed that the black dye is the best absorbing material to increase the still productivity [6]. Many studies [11,15] presented the effect of water flowing over the glass cover on the performance of a single basin solar still. The basin water depth is having significant effect on productivity of the basin solar still, where it was found that the daylight productivity decreases with an increase in water depth and the reverse is the case overnight due to the increased heat capacity of basin water with increasing depth [16].

In previous work, fins were used for increasing heat transfer rate from the basin liner of the still to the basin water. Velmurugan et al. [19,30] used fins for increasing the productivity of a liquid waste still where the single basin solar still was integrated with fin, black rubber, sand, pebble, and sponges. It was found that the evaporation rate increased by about 53% when fins were integrated at the basin plate. Performances of finned and corrugated absorber solar stills were also studied by Omara [27]. It was found that at quantity of saline water of 30 l, the productivity increased approximately by 40 and 21%, respectively, when finned and corrugated basin liners were used. The thermal performance of an ethanol solar still with finned plate was carried out by Ayuthaya et al. [31]. A basin solar still was integrated with a set of finned plate fitted in the still basin for distillation of a 10% V/V alcohol solution. It had six stainless-steel fins (fin size was $0.04\ m^3 \times 0.7\ m^3 \times 0.001\ m^3$) integrated to a black absorber. The results showed that the productivity of the modified solar still was increased by 15.5% compared to that of a conventional still (CS) [31]. Winter and summer performances of single sloped basin type solar still integrated with extended porous fins were studied by Srivastava and Agrawal [32]. The porous fins were made up of blackened old cotton rags partially dipped in the basin water, while the rest part of the fin extends above the basin water surface. Fifty-six percent higher daytime distillate and 48% higher for 24 h duration was obtained in the month of February over the CS.

Many factors affect the cost of distillate obtained from a solar desalination unit. Both capital and running (and so the total) costs are influenced by the unit size, site location, feed water properties, produced water quality, qualified staff availability, etc. The main economic advantages of solar desalination should not require much infrastructure, and it is simple to locally design, install, operate, and maintain. The better economic return on the investment depends on the production cost of the distilled water and its applicability [33–35].

The main purpose of this work is to design, fabricate, and investigate the thermal performance of a finned-basin liner single effect solar still. A transient mathematical model of the still was formulated to optimize the still performance. For the first time in the theoretical analysis, the effect of the fin shadow on the amount of solar radiation received by the still basin was taken into consideration. The performance of the modified still was compared with that of the conventional basin type solar still of identical dimensions and materials. Comparisons between experimental and theoretical results were performed. Comparisons of the obtained results with those presented in previous studies were also made. The cost analysis of the FBLS and CS has been performed on the basis of the prices of the raw materials (according to the Egyptian market) used in their construction.

2. Construction of solar stills

2.1. Conventional still

The CS is a single slope single basin solar still with a basin area of 1 m^2. The depth of the high-side wall of the still is 55 cm and the low-side height is 25 cm, as shown in Fig. 1. The whole basin surfaces were coated from inside with black paint to increase the absorptivity of solar radiation. The still was insulated from the bottom and side walls with foam (5-cm thick) to reduce the heat loss from the still to ambient air. The insulation layer was supported by a galvanized iron frame with thickness 0.1 cm. A black painted copper sheet (0.1-cm thick) was used as the still absorber plate. Since the still was investigated on typical summer days, the basin was covered with a glass sheet of 0.4-cm thickness inclined at 15° with horizontal, to maximize the amount of solar radiation incident on the still cover. The whole experiment setup was oriented to face south to receive maximum solar radiation. Fig. 2 shows a photograph of the constructed CS.

2.2. Finned-basin liner still

The CS was integrated with metallic fins (perpendicular to the distillate channel) to be used as extended surfaces. The fins were used to increase the basin liner surface area and improve the rate of heat transfer to the basin water. The finned-basin liner still (FBLS) (shown in Fig. 3(a)) has the same construction materials and dimensions of the CS except the flat copper

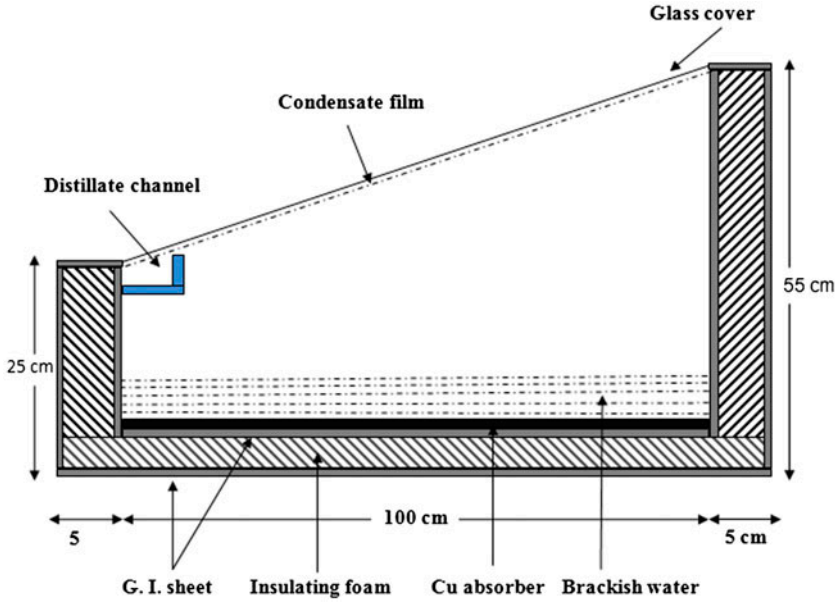

Fig. 1. A schematic of the CS.

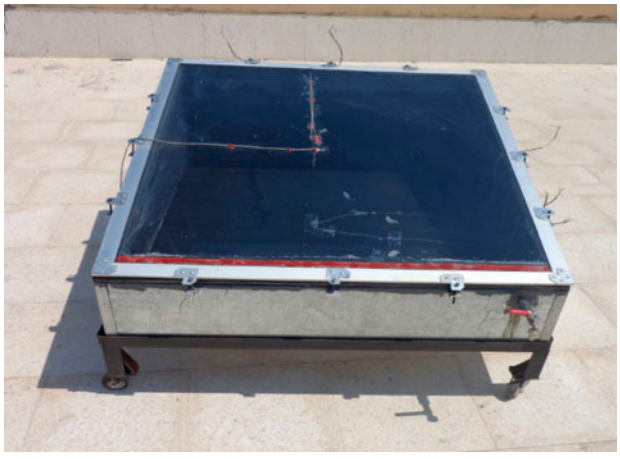

Fig. 2. A photograph of the constructed CS.

absorber was replaced by a black painted finned absorber with 14 fins. The fin has 4-cm height, 0.1-cm thick, and 6-cm pitch (the distance between two successive fins). Fig. 3(b) presents detailed dimensions of the fins. Fig. 4 shows a photograph of the modified still with fins (FBLS). Fig. 5 presents a photograph of the finned plate showing the shadow of the fins.

3. Mathematical models

The transient mathematical models of the conventional and modified stills are based on writing the energy balance equations for the various components of the stills. The energy balance equations of the basin liner, basin water, inner and outer surfaces of the glass cover of the CS were formulated and solved in a previous work [36]. However, in order to write the energy balance equations of the modified still (FBLS), the following assumptions are made: (i) Since the heat capacities of glass and foam are lower than that of water, the heat capacities of the glass cover and insulation are negligible. (ii) There is no temperature gradient across the basin water. This assumption is justified by taking a shallow depth of basin water of 4 cm. (iii) The side losses and glass reflectivity are negligible (the stills were insulated with 5-cm foam). (iv) The solar distiller units are air and vapor tight where the silicon rubber was used as a sealant during the construction of the stills.

3.1. For the outer surface of the glass cover

$$U_g A_g (T_{gi,f} - T_{go,f}) = h_{cgoa} A_g (T_{go,f} - T_a) + h_{rgos} A_g (T_{go,f} - T_s) \quad (1)$$

where U_g is the conductive heat transfer coefficient from inner to outer surface of the glass cover, given by:

$$U_g = K_g / x_g \quad (1a)$$

3.2. For the inner surface of the glass cover

$$I_t \alpha_g A_g + h_1 A_g (T_{w,f} - T_{gi,f}) = U_g A_g (T_{gi,f} - T_{go,f}) \quad (2)$$

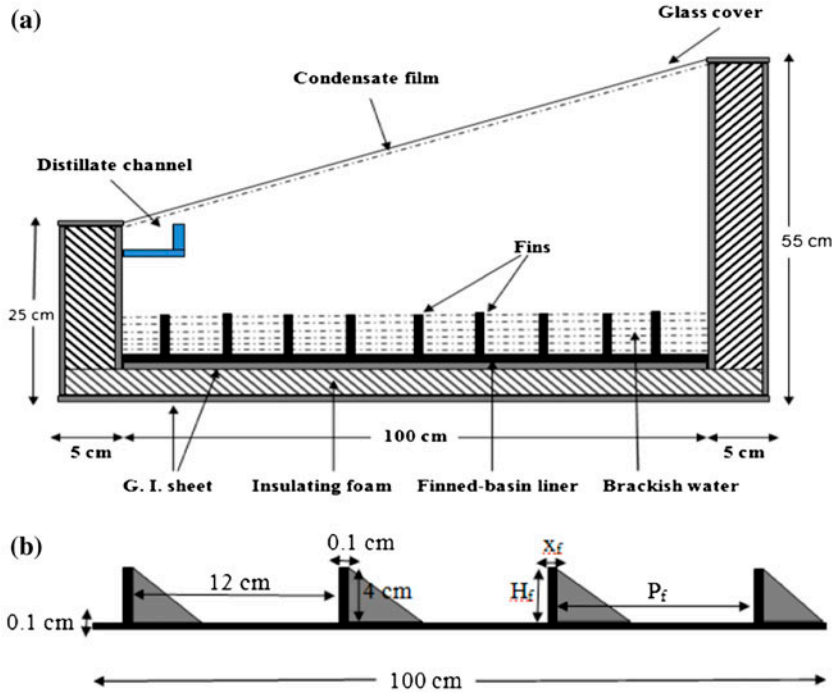

Fig. 3. (a) A schematic of the finned-basin liner still (FBLS) and (b) Detailed dimensions of the fins.

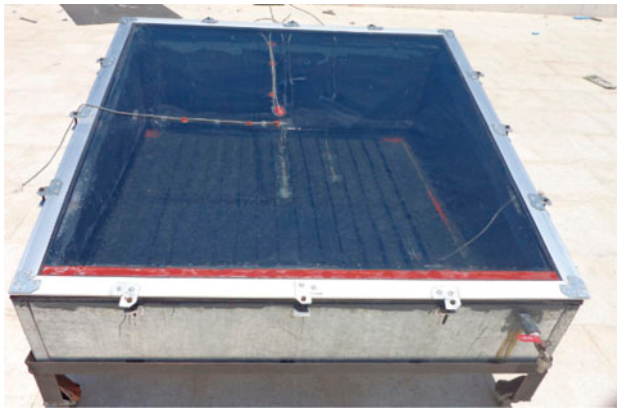

Fig. 4. A photograph showing the modified still with fins (FBLS).

Fig. 5. A photograph showing the shadow area of the fins.

where I_t is the global solar radiation intensity incident on the still cover. $h_1 = \left(h_{rwgi} + h_{cwgi} + h_{ewgi}\right)$ is the total internal heat transfer coefficient from the basin water to the inner surface of the glass cover and h_{rwgi}, h_{cwgi}, and h_{ewgi} are calculated using Dunkle correlations [37].

3.3. For the basin water

The fin shadow affects the amount of solar radiation received by the still basin; therefore, when writing the energy balance equations of the basin water and finned absorber of the FBLS, the fins shadow areas must be taken into account. In this work, the method described by Jaefarzadeh [38] was used to calculate the fins shadow area (A_{sh}). The shadow area due to one fin is given by the following equation [38]:

$$A_{sh} = H_f l_{sh} \sin\varphi + H_f l_{sh} \cos\varphi - l_{sh}^2 \sin\varphi \cos\varphi \quad (3)$$

with

$$\varphi = \sin^{-1}(\cos\theta_v / \sin\theta_i) \quad (3a)$$

where H_f is the height of the fin and l_{sh} is the shadow length of the fin. The formulas used for calculating the shadow area of the fins A_{sh} are given in the Appendix A. The total shadow area of the fins ($A_{sh,t}$) is, therefore,

$$A_{sh,t} = n_f A_{sh} \tag{4}$$

where n_f is the number of fins. On the basis of the above method used to calculate the shadow area, the energy balance equation for the basin water may be written as:

$$I_t \tau_g \alpha_w A_{w,eff} + h_3 (T_{pf} - T_{w,f}) = h_1 A_w (T_{w,f} - T_{gi,f}) + m_w C_w \frac{dT_{w,f}}{dt} \tag{5}$$

where $A_{w,eff} = A_w - A_{sh,t}$ is the unshaded area of basin water surface in the presence of fins and h_3 is the convective heat transfer coefficient from the finned-basin liner to basin water given by the following formula:

$$h_3 = (h_{p,eff} A_{p,eff} + h_{cfw} A_f \eta_f) \tag{6}$$

where $h_{p,eff}$ and h_{cfw} are the convective heat transfer coefficients, from the effective area of the basin liner $A_{p,eff}$ and fins surfaces with area A_f, respectively. $h_{p,eff}$ and h_{cfw} are given by the following equations [39]:

$$h_{p,eff} = 0.54 \frac{K_w}{ds} (Gr \cdot Pr)^{1/4} \tag{6a}$$

and

$$h_{cfw} = 0.8 \frac{K_w}{d_w} (Gr \cdot Pr)^{1/4} \left[1 + \left(1 + \frac{1}{\sqrt{Pr}} \right)^2 \right]^{-1/4} \tag{6b}$$

where $A_{p,eff} = n_f P_f l$ is the effective area of the plate with fins. $A_f = 2 n_f H_f l_f$ is the total surface area of the fins. η_f is the fin efficiency given as [40]:

$$\eta_f = \frac{\tanh \sqrt{2 h_{cfw} H_f / K_f x_f}}{2 h_{cfw} H_f / K_f x_f} \tag{7}$$

where K_f and x_f are the thermal conductivity and thickness of the fin. $d_w = m_w / \rho_w A_w$ is the depth of the basin water.

3.4. For the finned basin liner

The energy balance equation of the finned basin liner is given as

$$\tau_g \tau_w \alpha_p I_{pf} = h_3 (T_{pf} - T_{w,f}) + U_b A_p (T_{pf} - T_a) + m_{pf} C_p \frac{dT_{pf}}{dt} \tag{8}$$

where I_{pf} is the total solar radiation incident on the finned basin liner calculated as follows:

$$I_{pf} = \left(I_{f,w} \frac{A_f}{2} \right) + \left(I_{f,e} \frac{A_f}{2} \right) + (I_t A_{p,eff,sh}) \tag{8a}$$

where $I_{f,w}$ and $I_{f,e}$ are the total solar radiation intensities incident on west and east surfaces of the fin, respectively. m_{pf} is the total mass of the basin liner m_p and fins m_f given by the following equation:

$$m_{pf} = m_p + m_f = \rho_p (A_p x_p + n_f l H_f x_f) \tag{8b}$$

From Eqs. (1) and (2), we get:

$$T_{go,f} = \frac{h_{cgoaT_a} + h_{rgos} T_s + U_g T_{gi,f}}{h_2} \tag{9}$$

and

$$T_{gi,f} = \frac{U_g T_{go,f} + I_t \alpha_g + h_1 T_{w,f}}{U_g + h_1} \tag{10}$$

where $h_2 = U_g + h_{cgoa} + h_{rgos}$ is the total external heat transfer coefficient. Substituting $T_{go,f}$ and $T_{gi,f}$ and using Eqs. (9) and (10) and Eqs. (5) and (8) may be simplified as

$$M_1 \frac{dT_{w,f}}{dt} = -a_1 T_{w,f} + h_3 T_{pf} + X(t) \tag{11}$$

and

$$M_2 \frac{dT_{pf}}{dt} = -a_2 T_{pf} + h_3 T_{w,f} + Y(t) \tag{12}$$

The coefficients of Eqs. (11) and (12), viz. M_1, M_2, a_1, a_2, $X(t)$, and $Y(t)$ are given in the Appendix B. Eqs. (11) and (12) are solved analytically using the elimination technique [41], assuming that $X(t)$ and $Y(t)$ have average values $\overline{X(t)}$ and $\overline{Y(t)}$ over a time interval from zero to t and may be treated as constants. $\overline{X(t)}$ and $\overline{Y(t)}$ are functions of solar intensity and ambient temperature. The values of solar intensity and ambient temperature have been measured for specified time intervals and then their average values are calculated to be used for numerical calculations. Also, the heat transfer coefficients remain constants over the selected time interval [42]. From Eqs. (11), we have:

$$T_{pf} = \frac{1}{h_3}\left[M_1 \frac{dT_{w,f}}{dt} + a_1 T_{w,f} - \overline{X(t)}\right] \quad (13)$$

By substitution of T_{pf} from Eq. (13) into Eq. (12), one may get:

$$M_1 M_2 \frac{d^2 T_{w,f}}{dt^2} + (M_2 a_1 + M_1 a_2)\frac{dT_{w,f}}{dt} + (a_1 a_2 - h_3^2) T_{w,f} = a_2 \overline{X(t)} + h_3 \overline{Y(t)} \quad (14)$$

The general solution of Eq. (14) may be given as [43]:

$$T_{w,f} = T_{comp} + T_{par} \quad (15)$$

where T_{comp} is the complimentary solution and T_{par} is the particular solution. The complimentary solution is given by:

$$T_{comp} = C_1 e^{\Delta_+ t} + C_2 e^{\Delta_- t} \quad (16)$$

with

$$\Delta_\pm = \frac{\left[-(M_2 a_1 + M_1 a_2) \pm \sqrt{(M_2 a_1)^2 + (M_1 a_2)^2 - 2M_1 M_2 (a_1 a_2 - 2h_3^2)}\right]}{2M_1 M_2} \quad (17)$$

where C_1 and C_2 are constants to be determined using the following initial conditions at $t = 0$.

$$T_{w,f} = T_{w,fi} \quad \text{and} \quad T_{pf} = T_{pfi} \quad (18)$$

where $T_{w,fi}$ and T_{pfi} are the initial temperatures of the basin water and basin liner, respectively. Since the nonhomogeneous portion of Eq. (14) is a constant, T_{par} may also be assumed to be a constant [43]. Substituting Eq. (15) into Eq. (14) we get:

$$T_{par} = \frac{a_2 \overline{X(t)} + h_3 \overline{Y(t)}}{a_1 a_2 - h_3^2} \quad (19)$$

The general solution of the Eq. (14) then becomes

$$T_{w,f} = C_1 e^{\Delta_+ t} + C_2 e^{\Delta_- t} + T_{par} \quad (20)$$

Then T_{pf} from Eq. (13) can be obtained as

$$T_{pf} = \frac{1}{h_3}\left[C_1 e^{\Delta_+ t}(M_1 \Delta_+ + a_1) + C_2 e^{\Delta_- t}(M_1 \Delta_- + a_1) + a_1 T_{par} - \overline{X(t)}\right] \quad (21)$$

Applying the initial conditions, Eq. (18), into the last two equations, the constants C_1 and C_2 are obtained as:

$$C_1 = \frac{\left[T_{w,fi}(M_1 \Delta_- + a_1) - T_{pfi} h_3 - M_1 \Delta_- T_{par} - \overline{X(t)}\right]}{M_1(\Delta_- - \Delta_+)} \quad (22)$$

and

$$C_2 = \frac{\left[T_{pfi} h_3 - T_{w,fi}(M_1 \Delta_+ + a_1) + M_1 \Delta_+ T_{par} + \overline{X(t)}\right]}{M_1(\Delta_- - \Delta_+)} \quad (23)$$

The hourly productivity of the FBLS is defined as:

$$P_{h,f} = h_{ewgi}\left(T_{w,f} - T_{gi,f}\right) \times \frac{3,600}{L_w} \quad (24)$$

The daily productivity and efficiency of the FBLS can be written as:

$$P_{d,f} = \sum_{24\,h} P_{h,f} \quad (25)$$

and

$$\eta_{d,f} = \left[\frac{(P_{d,f} L_{av})}{(A_p \sum I_t)\Delta t}\right] \times 100\% \quad (26)$$

where L_{av} is the daily average of the latent heat of vaporization of water and Δt is the time interval during which the solar radiation is measured.

4. Experiments and numerical calculations

In order to study the effect of climatic, operational, and design parameters on the performance of the CS and FBLS, experiments were carried out during typical days of June 2014. The system was oriented to face south to maximize the solar radiation received by the

still. The global solar radiation incident on a horizontal surface was measured using an Eppley-Precession Spectral Pyranometer (EPSP) coupled to an Instantaneous Solar Radiation Meter Model No. 455. Calibrated NiCr-Ni thermocouples connected to a FLUKE 73 digital multimeter were used to measure the temperatures of different elements of the still every hour. Two thermocouples were fixed in the basin water at depths of about 1 and 3 cm to measure the average temperature of the basin water. Other thermocouples were fixed at the upper and lower surfaces of the glass cover while another one was used to record the temperature of the absorber plate. The ambient temperature was also recorded using a mercury thermometer. To carry out the various experiments on the CS and FBLS, two models were constructed and tested under the same outdoor conditions. The FBLS was tested with 14 fins and depth of water of 4 cm.

To validate the proposed mathematical model, numerical calculations were performed employing the climatic conditions recorded during the experimental test of the still; where a computer program was developed based on the solution of the energy balance equations of the still elements. The various internal and external heat transfer coefficients were calculated. Hourly values of different temperatures and productivity of the still were then calculated. The following values of the different parameters were used; $\alpha_g = 0.05$, $\tau_g = \alpha_p = 0.83$, $\alpha_g = 0.05$, $\tau_w = 0.36 - 0.08 \ln(d_w)$ [44], $A_p = A_w = 1\ m^2$, $A_g = 1.035\ m^2$ when $\beta = 15^\circ$, $x_b = x_s = 0.05$ m, $x_g = 0.004$ m, $x_p = 0.001$ m, $k_g = 0.78$ (W/m K), $k_w = 0.6405$ (W/m K), $k_b = k_s$ (foam) = 0.025 (W/m K), $\sigma = 5.669 \times 10^{-8}(W/m^2\ K^4)$, $\varepsilon_g = 0.88$, $V = 2$ m/s, $C_w = 4{,}190$ (J/kg K). The daily productivity and efficiency of the still were then calculated using Eqs. (25) and (26).

4.1. Experimental uncertainty

In general, the result of any measurement of physical quantity must include both the value itself (best value) and its error (uncertainty). The result is usually quoted in the form:

$$x = x_{best} \pm \Delta x \tag{27}$$

where x_{best} is the best estimate of what we believe is a true value of the physical quantity and Δx is the estimate of absolute error (uncertainty). Errors and uncertainties in the experiments can arise from instruments selection, condition, calibration, environment, observation, reading, and test planning. In experiments in solar still, the temperatures, mass of fresh water, and solar radiation were measured with appropriate instruments. During the measurement of these parameters, the uncertainties that occurred were presented in Table 1 and shown as vertical error bars in the curves presented in Section. 5 "Results and discussions". For an experimental parameters x_i, uncertainties estimation was made using the following equation [45]:

$$W = \sqrt{\sum_{i=1}^{n} x_i^2} \tag{28}$$

5. Results and discussions

The conventional and modified stills are investigated theoretically and experimentally on typical days of June 2014. The obtained results are summarized in the following sections.

5.1. Temperatures distribution

Hourly variations of the solar radiation incident on the still cover I_t as well as measured temperatures of ambient T_a, basin water T_w, basin liner T_p, inner T_{gi}, and outer T_{go} surfaces of the glass cover for the CS on 11 June 2014 when $m_w = 40$ kg is shown in Fig. 6a. From the results of Fig. 6a, it is seen that the solar intensity increases with the time of day to show its maximum value of 928.33 W/m^2 at 1.0 PM. The T_w, T_p, T_{gi}, and T_{go} are exhibiting the same behavior of solar radiation with shift of peak positions due to the thermal inertia of the still elements and basin water. The maximum values of T_w, T_p, T_{gi}, and T_{go}

Table 1
The uncertainties during the measurements of the parameters

Instrument	Accuracy	Range
Thermocouple	±0.625℃	0–100℃
Ambient air temperature	±0.5℃	0–100℃
Eppley-Precession Spectral Pyranometer	±1.0 W/m^2	0–1,200 W/m^2
Productivity measurement	±10.0 g	0.1–600 g
Time measurement	0.016 min	60 min

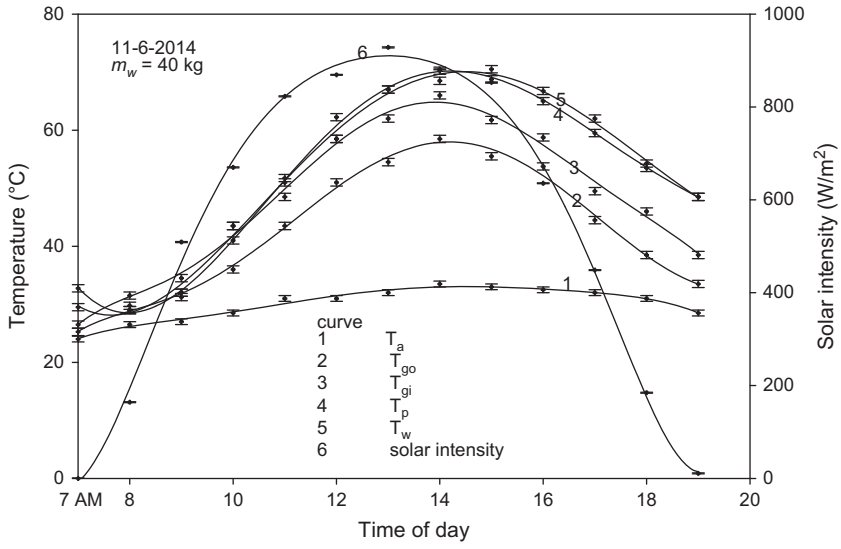

Fig. 6a. Hourly variations of solar intensity and measured temperatures for different elements of the CS on 11 June 2014.

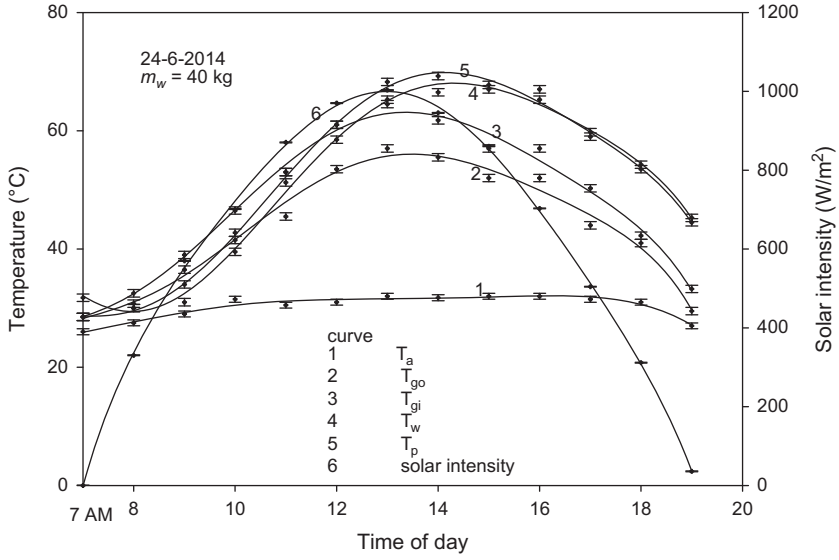

Fig. 6b. Hourly variations of solar intensity and measured temperatures for different elements of the FBLS on 24 June 2014.

are obtained as 70.25, 70.5, 66, and 58.5°C, respectively. The basin liner temperature is slightly higher than that of basin water during sunshine hours. These results prove that the predominate mode of heat transfer from the basin liner to the basin water is the convective mode.

Fig. 6b presents variations of measured temperatures of the finned plate still (FBLS) on 24 June 2014 when n_f = 14 and m_w = 40 kg (the depth of basin water equals the fin height). From Fig. 6b, it is observed that the solar radiation intensity increases with the time of day to show its maximum value of 1,002.96 W/m^2 at 1.0 PM. The temperatures of all elements of the FBLS show similar behavior as those of the CS; except, there is a shift of peak positions of basin liner and basin water temperatures (as examples) compared with those of the CS. The latter results are occurred because the thermal inertia of the basin liner of the modified still is higher that of than the CS; more material was used for fabricating the finned basin liner. The maximum values of $T_{w,f}$, $T_{p,f}$, $T_{gi,f}$, and $T_{go,f}$ are obtained as 75, 69.25, 64.5, and 57°C, respectively. It is obvious

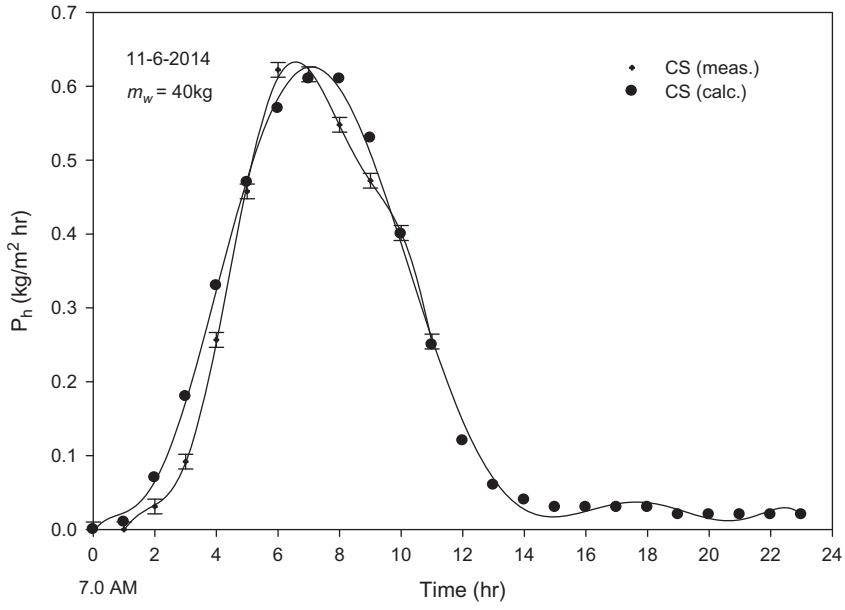

Fig. 7a. Comparisons between measured and calculated hourly productivity of the CS.

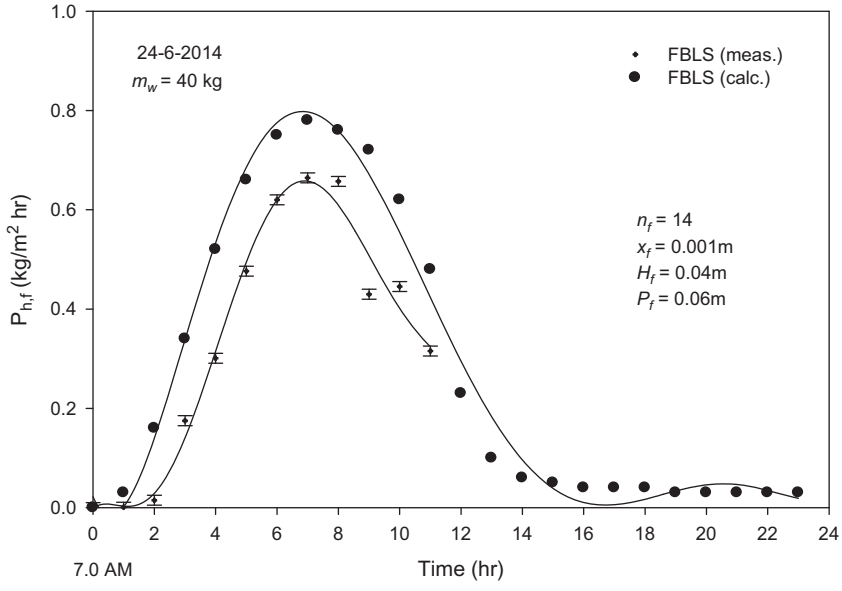

Fig. 7b. Comparisons between measured and calculated hourly productivity of the FBLS.

that the modified still (FBLS) operates at higher temperatures compared to the CS due to the increased heat transfer area and heat transfer rate from the finned basin liner to the basin water. The measured daily productivities of the conventional and modified stills are found to be 4.235 and 4.802 (kg/m^2 d) with daily efficiencies of 42.36 and 55.37%, respectively. The relative percentage improvement ratios in daily productivity and efficiency are obtained as 11.8 and 23.5% when the conventional basin liner is replaced by a finned plate basin liner.

5.2. Comparisons between experimental and theoretical results

In order to validate the proposed theoretical models, comparisons between measured and calculated hourly productivity P_h were performed.

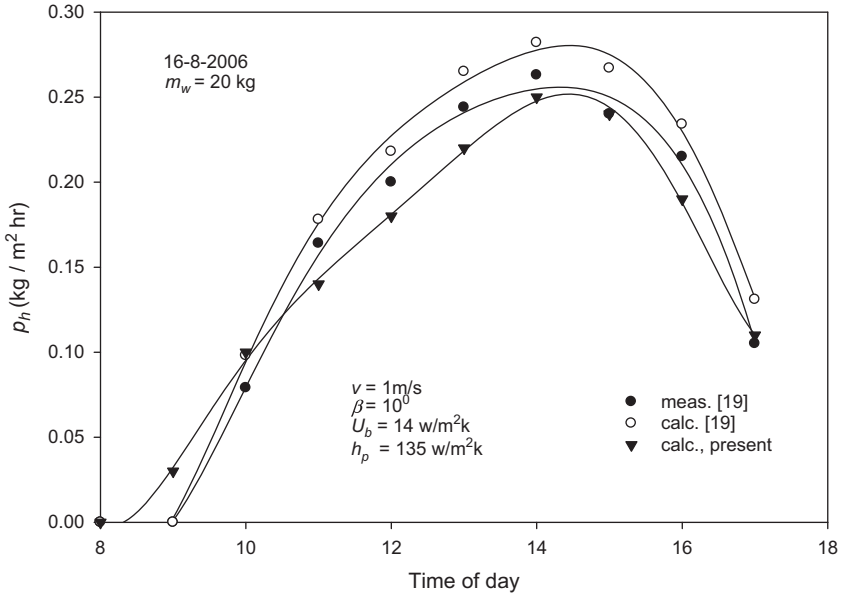

Fig. 8a. Comparisons between calculated values of P_h and the measured and calculated values of Velmurugan et al. [19] for the CS when m_w = 20 kg.

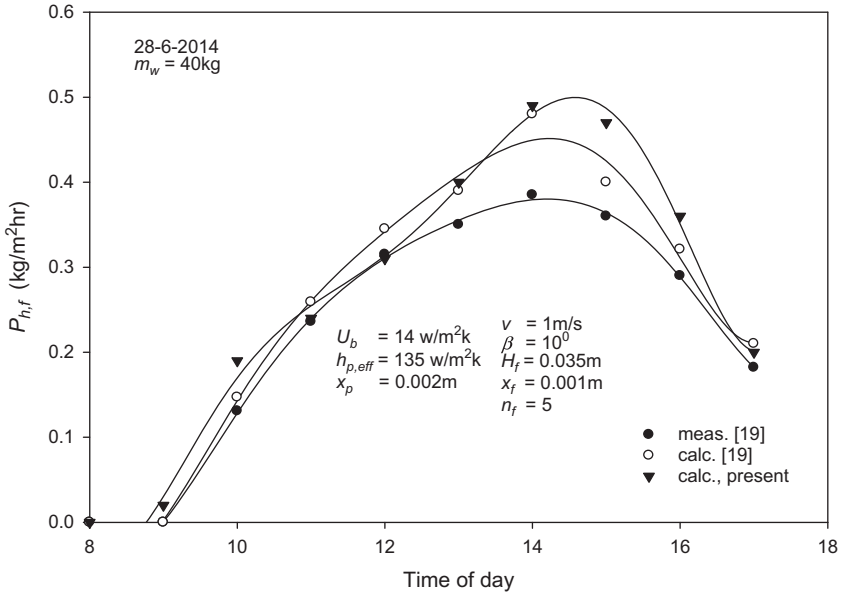

Fig. 8b. Comparisons between calculated values of $P_{h,f}$ and the measured and calculated values of Velmurugan et al. [19] for the FBLS when m_w = 20 kg.

Fig. 7a summarizes comparisons between measured and calculated P_h of the CS on 11 June 2014 when m_w = 40 kg. The maximum value of the measured P_h equals 0.622 (kg/m^2 h) in comparison to 0.610 (kg/m^2 h) that obtained by numerical calculations for the day 11 June 2014. The daily average of measured and calculated P_h equals 0.313 and 0.320 (kg/m^2 h), respectively. The measured and calculated daily productivity P_d for the CS are calculated from the values of P_h to be 4.235 and 4.475 (kg/m^2 d), respectively, with a relative percentage deviation between theoretical and experimental result of 5.36%.

Comparisons between measured and calculated hourly productivity $P_{h,f}$ of the FBLS on 24 June

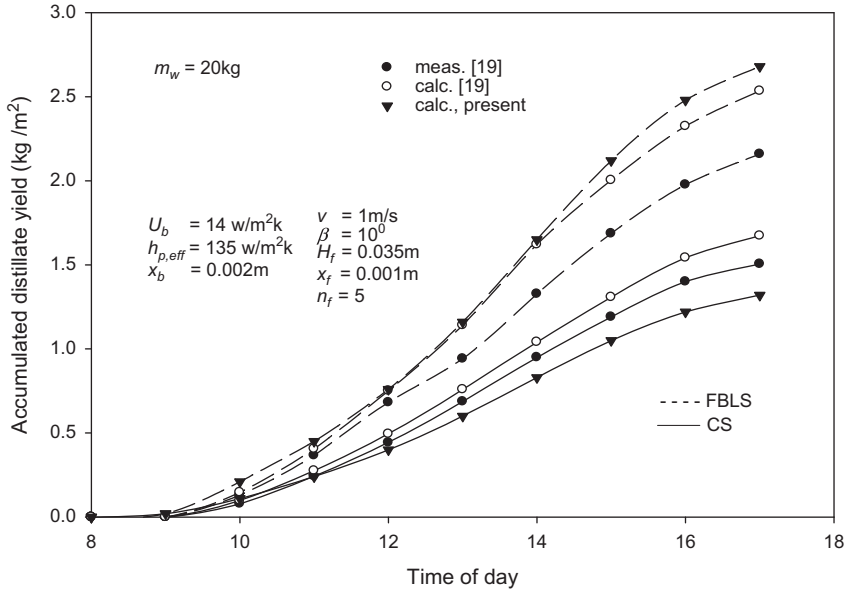

Fig. 9. Comparisons of the measured and calculated accumulated distillate yield [19] with the present calculated values for the CS and FBLS.

2014when $n_f = 14$ and $m_w = 40$ kg is presented in Fig. 7b. The maximum value of the measured $P_{h,f}$ equals 0.664 (kg/m^2 h) in comparison to 0.780 (kg/m^2 h) obtained by numerical calculations. It is evident from the results of Fig. 7a that the agreement between measured and calculated productivities of the CS is excellent; however, there is some difference between measured and calculated productivities of the modified still may be due to the following reasons: (i) The temperature distributions inside the basin water is neglected, (ii) Uncertainties in the correlations used for calculating different heat transfer coefficients and solar intensity incident on the still cover, east and west surfaces of the fins, (iii) Uncertainty in the method used for calculations of the fins shadow area may represent another source of error, and (iv) The time required for preheating the still elements is not taken into consideration in the mathematical analysis.

5.3. Comparisons with previous work

For further validation of the theoretical models proposed for the CS and FBLS, comparisons between the obtained theoretical results and those measured/calculated in previous work [19] are also made.

Fig. 8a shows comparisons between calculated values of P_h and the corresponding measured and calculated values of Velmurugan et al. [19] for the CS on 16 August 2006 when $m_w = 20$ kg. It is seen that the values of P_h calculated using the present model for the CS are in good agreement with those measured and calculated values by Velmurugan et al. [19]. It is found that the present calculated value of daily productivity P_d equals1.79 (kg/m^2 d) compared to the measured and calculated values of 1.88 and 2.07 (kg/m^2 d) found in Ref. [19]. Comparisons between our results and those measured or calculated values of Velmurugan et al. [19] for the finned plate solar still when $n_f = 5$ and $m_w = 20$ kg, are also made and the results are presented in Fig. 8b.

It is found that the values of the daily productivity P_d were calculated and measured by Velmurugan et al. [19] for the FBLS are 3.09 and 2.81 (kg/m^2 d), respectively, compared to our calculated value of $P_{d,f}$ of 3.18 (kg/m^2 d). The relative percentage difference between the present results and those of Velmurugan et al. [19] is found in the range 2.8–11.6%.

Fig. 9 presents comparisons between measured and calculated accumulative distillate yield of Velmurugan et al. [19] and the corresponding values of the calculated results obtained using the present theoretical models for the CS and FBLS when $m_w = 20$ kg. Again the agreement between our results and those presented in the literature [19] is satisfactory. The deviation between the present results of accumulative productivity and Velmurugan et al. [19] results due to the same reasons mentioned during the discussion of Fig. 7b.

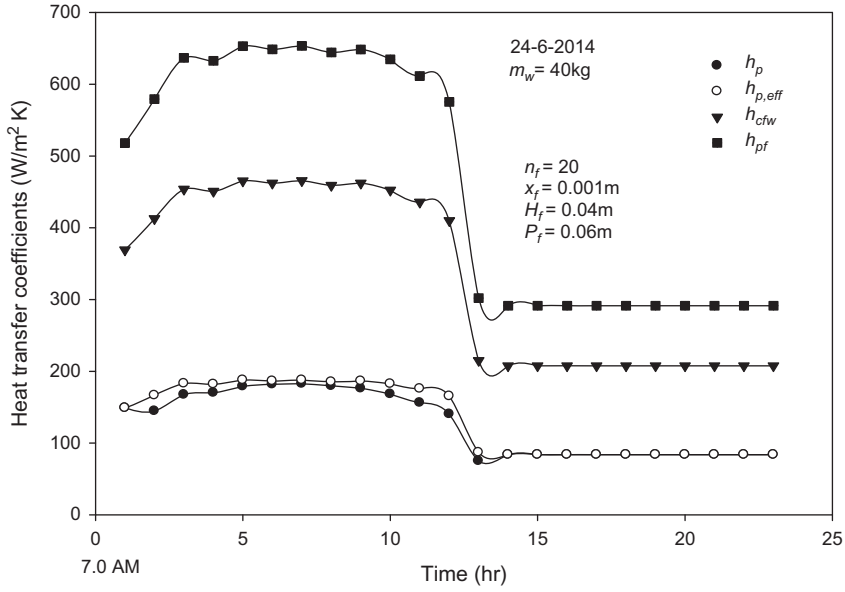

Fig. 10a. Comparisons between calculated convective heat transfer coefficients from basin liner to basin water in case of the CS and FBLS on 24 June 2014.

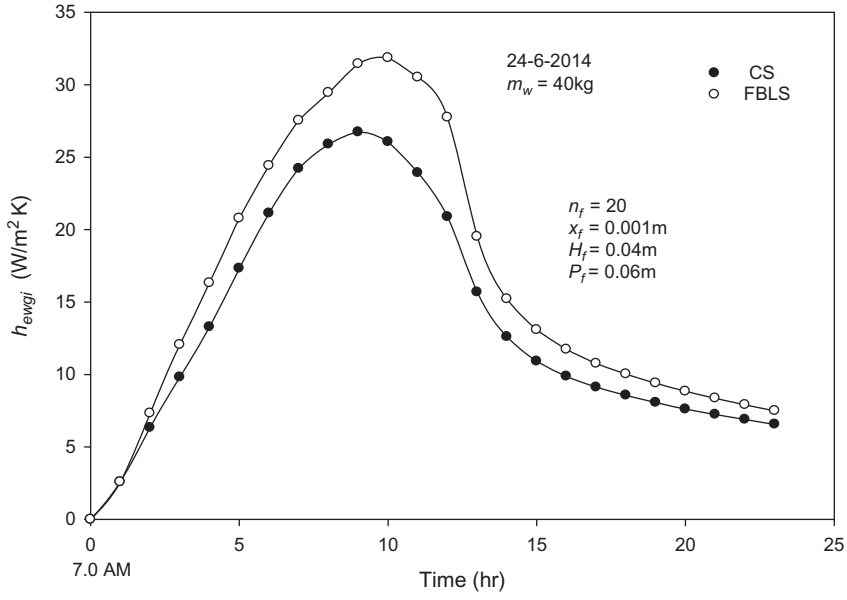

Fig. 10b. Comparisons between calculated evaporative heat transfer coefficients h_{ewgi} for the CS and FBLS on 24 June 2014.

5.4. Heat transfer coefficients

Fig. 10a explains comparisons between the calculated convective heat transfer coefficients from the basin liner to the basin water for conventional and finned plate stills on 24 June 2014 when $n_{\mathrm{f}} = 14$ and $m_{\mathrm{w}} = 40$ kg. It is observed that the convective heat transfer coefficients for the FBLS from the effective area of the finned plate to basin water $h_{\mathrm{p,eff}}$ is slightly higher than that for the CS h_{p} as expected; however, the total convective heat transfer coefficients from the finned plate to the basin water h_{pf} ($h_{\mathrm{pf}} = h_{\mathrm{p,eff}} + h_{\mathrm{cfw}}$) is considerably higher than that of the CS h_{p} ($h_{\mathrm{cfw}} = 0$, plate without fins), because for the finned still there is

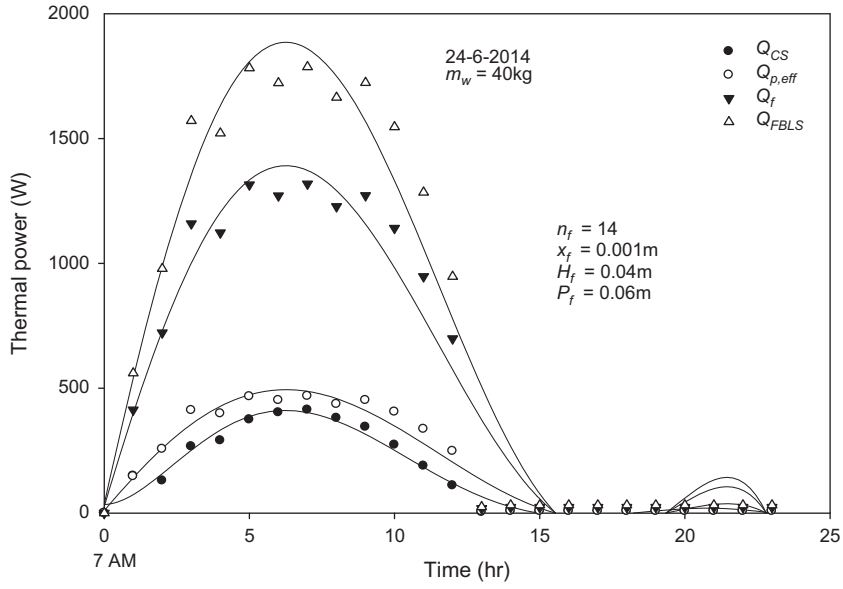

Fig. 11. Comparisons between calculated thermal powers for the CS and FBLS.

an additional heat transfer source from the fin surfaces to the basin water as is shown by the coefficient h_{cfw} in Fig. 10a. The maximum values of $h_{p,eff}$ and h_{cfw} for the FBLS are obtained as 187.81 and 465.52 W/m^2 K, respectively. Therefore, the maximum values of total convective heat transfer coefficients to the basin water for the finned and CSs are found to be 653.33 and 182.64 W/m^2 K, respectively. These results indicate that h_{pf} is about 3.6 times higher than h_p. The increase in the convective heat transfer coefficients from the finned plate is mainly the reason for the improvement in the productivity of the FBLS. Consequently, the calculated evaporative heat transfer coefficient h_{ewgi} in case of the FBLS shows higher values than those of the CS during all time of the day as seen in Fig. 10b. From the results of Fig. 10b, it is found that the maximum values of h_{ewgi} for the CS and FBLS are 26.73 and 31.85 W/m^2 K, respectively. The behavior of h_{ewgi} (Fig. 10b) is identical to that of hourly productivity (see Fig. 7) because h_{ewgi} is the main parameter affecting the solar still productivity.

Fig. 11 shows the rate of heat transfer (thermal power) from the basin liner to basin water for the conventional and finned plate stills on 24 June 2014 when $n_f = 14$ and $m_w = 40$ kg. It is noticed that the thermal power from the effective area of the finned plate $\dot{Q}_{p,eff}$ and the fin surfaces $\dot{Q}_f$ and hence, their sum $\dot{Q}_{FBLS}$ for the FBLS are higher than those for the CS $\dot{Q}_{CS}$. The maximum values of the $\dot{Q}_{p,eff}$, $\dot{Q}_f$, $\dot{Q}_{FBLS}$, and $\dot{Q}_{CS}$ are obtained as 468.25, 1,318.38, 1,786.63, and 413.19 W, respectively; whereas, their average values are found to be 190.31, 535.83, 726.14, and 142.15 W, respectively. The latter results attributed to the increased heat transfer area and the enhanced heat transfer coefficients to the basin water in case of the FBLS compared with those of the CS. Effect of fin configuration parameters on the still performance was investigated by El-Sebaii et al. [46]. It was found that the productivity of the finned plate solar still (FBLS) increases with increasing the fin height; however, it decreases with increasing the fin thickness and fin number. A daily productivity of 5.377 (kg/m^2 d) was obtained when n_f, H_f, and x_f equal 7, 0.04 and 0.001 m, respectively. Numerical results indicated that the cost of 1 L of distillate water equals 0.28 LE which is competitive with all prices of production of one liter of fresh water obtained from different designs of solar stills tested in different places of the world [33].

6. Conclusions

The performance of the conventional (CS) and finned (FBLS) solar stills was investigated. The experimental and theoretical results showed that the thermal performance of the CS can be improved by integrating fins to the basin liner of the still. It was found that, on a typical day of June, the daily productivities of the conventional and modified stills are 4.235 and 4.802 (kg/m^2 d) with daily efficiencies of 42.36 and 55.37%, respectively. The integrated fins at the base of the solar still gave 11.8 and 23.5% increase in the amount of distilled water produced and daily efficiency compared with a CS. The convective heat transfer coefficient from the finned plate is increased by 3.6 times

compared to the case without fins. The agreement between measured and calculated results is fairly good, also the present results agree well with those found in the literature with a relative percentage error in the range 2.8–11.6%.The proposed mathematical model for the FBLS can be used for predicating the thermal performance of single effect finned solar stills with a reasonable accuracy.

Nomenclature

A	—	surface area (m^2)
$A_{p,eff,sh}$	—	effective area of the plate in the presence of shadow due to fins (m^2)
B	—	width of the still (m)
C	—	conventional still
d	—	depth (m)
d*s*	—	standard length of the absorber plate (m)
FBLS	—	finned-basin liner still
Gr	—	Grashof number
H	—	height (m)
h	—	heat transfer coefficient (W/m^2 K)
I	—	global solar radiation intensity (W/m^2)
K	—	thermal conductivity (W/m K)
L	—	length of the still (m)
n	—	refractive index of water
n_d	—	day of the year
n_f	—	number of the fins
P	—	productivity (kg/m^2)
P_f	—	pitch, the distance between two successive fins (m)
Pr	—	Prantdl number
$\dot{Q}$	—	thermal power (W)
t	—	desired time period (s)
T	—	temperature (K)
U	—	heat loss coefficient (W/m^2 K)
V	—	wind speed (m/s)
x	—	thickness (m)
z	—	local time

Greeks

α	—	absorptivity
β	—	inclination angle of the glass cover of the still with respect to horizontal (°)
γ	—	surface azimuth angle (°)
δ	—	angle of declination (°)
	—	emissivity
η	—	efficiency (%)
θ_i	—	angle of incidence of direct radiation to a horizontal plane with normal (Zenith angle) (°)
θ_v	—	angle of refraction (°)
ρ	—	density (kg/m^3)
σ	—	Stefan–Boltzmann's constant (W/m^2 K^4)
τ	—	transmissivity
φ	—	latitude of location (°)
ω	—	hour angle (°)

Subscripts

a	—	ambient
av	—	average
b	—	back insulting material
c	—	convective
d	—	daily
e	—	evaporative, east
eff	—	effective
f	—	fins
g	—	glass
h	—	hourly
i	—	inner
o	—	outer
p	—	absorber plate (basin liner)
pf	—	finned-basin liner
r	—	radiative
s	—	sky
sh	—	shadow
t	—	tilted, total
w	—	water, west

References

[1] T. Rajaseenivasan, K.K. Murugavel, T. Elango, R.S. Hansen, A review of different methods to enhance the productivity of the multi-effect solar still, Renewable Sustainable Energy Rev. 17 (2013) 248–259.

[2] M. Feilizadeh, M. Soltanieh, K. Jafarpur, M.R.K. Estahbanati, A new radiation model for a single-slope solar still, Desalination 262 (2010) 166–173.

[3] G.O.G. Lof, J.A. Eibling, J.W. Bloemer, Energy balances in solar distillation, AICHE J. 7 (1967) 641–649.

[4] P.I. Cooper, Digital simulation of transient solar still processes, Sol. Energy 12 (1969) 333.

[5] M.S. Sodha, A. Kumar, G.N. Tiwariand, R.C. Tyagi, Simple multiple wick solar still: Analysis and performance, Sol. Energy 26 (1981) 127–131.

[6] A.K. Rajvanshi, Effect of various dyes on solar distillation, Sol. Energy 27 (1981) 51–65.

[7] V.B. Sharma, S.C. Mullick, Estimation of heat transfer coefficients, the upward heat flow and evaporation in a solar still, Sol. Energy Transf. ASME 113 (1991) 36–41.

[8] G.N. Tiwari, J.M. Thomas, Emran Khan,Optimisation of glass cover inclination for maximum yield in a solar still, Heat Recovery Syst. CHP 14 (1994) 447–455.

[9] A.N. Minasian, A.A. Al-Karaghouli, An improved solar still: The wick-basin type, Energy Convers. Manage. 36 (1995) 213–217.

[10] S. Kumar, G.N. Tiwari, Estimation of convective mass transfer in solar distillation systems, Sol. Energy 57 (1996) 459–464.

[11] B.A.K. Abu-Hijleh, Enhanced solar still performance using water film cooling of the glass cover, Desalination 107 (1996) 235–244.

[12] B.A. Akash, M.S. Mohsen, O. Osta, Y. Elayan, Experimental evaluation of a single-basin solar still using different absorbing materials, Renewable Energy 14 (1998) 307–310.

[13] A.A. El-Sebaii, Effect of wind speed on some designs of solar stills, Energy Convers. Manage. 41 (2000) 523–538.
[14] A.S. Nafey, M. Abdelkader, A. Abdelmotalip, A.A. Mabrouk, Solar still productivity enhancement, Energy Convers. Manage. 42 (2001) 1401–1408.
[15] V. Bapeshwar, G.N. Tiwari, Effect of water flow over the glass on the performance of a solar still coupled with a flat plate solar collector, Sol. Energy 2 (1984) 277–288.
[16] S. Aboul-Enein, A.A. El-Sebaii, E. El-Bialy, Investigation of a single-basin solar still with deep basins, Renewable Energy 14 (1998) 299–305.
[17] B.A. Abu-Hijleh, H.M. Rababa'h, Experimental study of a solar still with sponge cubes in basin, Energy Convers. Manage. 44 (2003) 1411–1418.
[18] A.K. Tiwari, G.N. Tiwari, Effect of water depths on heat and mass transfer in a passive type solar still: In summer climatic condition, Desalination 195 (2006) 78–94.
[19] V. Velmurugan, M. Gopalakrishnan, R. Raghu, K. Srithar, Single basin solar still with fin for enhancing productivity, Energy Convers. Manage. 49 (2008) 2602–2608.
[20] S.K. Shukla, A.K. Rai, Analytical thermal modeling of double slope solar still by using inner glass cover temperature, Therm. Sci. 12 (2008) 139–152.
[21] H. Tanaka, Experimental study of a basin type solar still with internal and external reflectors in winter, Desalination 249 (2009) 1–8.
[22] A.A. El-Sebaii, A.A. Al-Ghamdi, F.S. Al-Hazmi, A.S. Faidah, Thermal performance of a single basin solar still with PCM as storage medium, Appl. Energy 86 (2009) 1187–1195.
[23] M. Sakthivel, S. Shanmugasundaram, T. Alwarsamy, An experimental study on regenerative solar still with energy storage medium—Jute cloth, Desalination 264 (2010) 24–31.
[24] M.S.E. Khaled, Improving the performance of solar still using vibratory harmonic effect, Desalination 251 (2010) 3–11.
[25] K. Kalidasa Murugavel, K. Srithar, Performance study on basin type double slope solar still with different wick materials and minimum mass of water, Renewable Energy 36 (2011) 612–620.
[26] N. Setoodeh, R. Rahimi, A. Ameri, Modeling and determination of heat transfer coefficient in a basin solar still using CFD, Desalination 268 (2011) 103–110.
[27] Z.M. Omara, Performance of finned and corrugated absorbers solar stills under Egyptian conditions, Desalination 277 (2011) 281–287.
[28] P.K. Srivastava, S.K. Agrawal, Experimental investigation of some design and operating parameters of basin type still, Int. J. Emergy Technol. Adv. Eng. 2 (2012) 225–230.
[29] P.K. Srivastava, S.K. Agrawal, Experimental and theoretical analysis of single sloped basin type solar still consisting of multiple low thermal inertia floating porous absorbers, Desalination 311 (2013) 198–205.
[30] V. Velmurugan, C.K. Deenadayalan, H. Vinod, K. Srithar, Desalination of effluent using fin type solar still, Energy 33 (2008) 1719–1727.
[31] R.P.N. Ayuthaya, P. Namprakai, W. Ampun, The thermal performance of an ethanol solar still with fin plate to increase productivity, Renewable Energy 54 (2013) 227–234.
[32] P.K. Srivastava, S.K. Agrawal, Winter and summer performance of single sloped type solar still integrated with extended porous fins, Desalination 319 (2013) 73–78.
[33] H.E.S. Fath, M. El-Samanoudy, K. Fahmy, A. Hassabou, Thermal-economic analysis and comparison between pyramid-shaped and single-basin solar still configurations, Desalination 159 (2003) 69–79.
[34] S. Kumar, G.N. Tiwari, Life cycle cost analysis of single slope hybrid (PV/T) active solar still, Appl. Energy 86 (2009) 1995–2004.
[35] J. Govind, G.N. Tiwari, Economic analysis of some solar energy systems, Energy Convers. Manage. 24 (1984) 131–135.
[36] A.A. El-Sebaii, M. Al-Dossari, A mathematical model of single basin solar still with an external reflector, Desalin. Water Treat. 26 (2011) 250–259.
[37] R.V. Dunkle, Solar water distillation: The roof type still and a multiple effect diffusion still, Int. Dev. Heat Transfer, University of Colorado, Part 5 (1961) 895–902.
[38] M.R. Jaefarzadeh, Thermal behavior of a small salinity-gradient solar pond with wall shading effect, Sol. Energy 77 (2004) 281–290.
[39] N.M. Ozisik, Heat Transfer, McGraw-Hill, New York, NY, 1988.
[40] H.M. Yeh, C.D. Ho, J.Z. Hou, Collector efficiency of double-flow solar air heaters with fins attached, Energy 27 (2002) 715–727.
[41] W.E. Boyce, R.C. Diprima, Elementary differential equations and boundary value problems, second ed., Wiley and Sons, New York, NY, 1969.
[42] V.B. Sharma, S.C. Mullick, Calculation hourly output of a solar still, ASME Trans. Solar Energy Eng. 115 (1993) 231–236.
[43] R. Chandra, V.K. Goel, B.C. Raychaudhuri, Performance comparison of two-pass modified reverse flat-plate collector with conventional flat-plate collectors, Energy Convers. Manage. 23 (1983) 177–184.
[44] M. Fishenden, O.A. Saunders, An Introduction to Heat Transfer, Oxford University Press, Oxford, 1950.
[45] J.P. Holman, Experimental Methods for Engineers, sixth ed., McGraw-Hill, Singapore, 1994.
[46] A.A. El-Sebaii, M.R.I. Ramadan, S. Aboul-Enein, M. El-Naggar, Effect of fin configuration parameters on single basin solar still performance, Desalination 365 (2015) 19–24.

Appendix A

Mathematical formulas for the various terms of Eqs. (3) and (3a) that are used for calculating the shadow area A_{sh}:

$$\cos\theta_i = \cos\delta\cos\phi\cos\omega + \sin\delta\sin\phi \tag{A1}$$

$$\delta = 23.45\sin\left[\frac{360(284+n_d)}{365.25}\right] \tag{A2}$$

$$\omega = \frac{2\pi(z-12)}{24} \tag{A3}$$

$$\cos\theta_v = -\sin\delta\cos\phi\cos\gamma + \cos\delta\sin\phi\cos\gamma\cos\omega + \cos\delta\sin\gamma\sin\omega \quad \text{(A4)}$$

$$\sin\theta_r = \frac{\sin\theta_i}{n} \quad \text{(A5)}$$

Appendix B

The coefficients of Eqs. (11) and (12) are given by:

$$M_1 = m_w C_w \quad \text{(B1)}$$

$$M_2 = m_{pf} C_p \quad \text{(B2)}$$

$$a_1 = h_3 + h_1 A_w - \frac{h_1^2 A_w}{h_1 + U_g} \quad \text{(B3)}$$

$$a_2 = h_3 + U_b A_P \quad \text{(B4)}$$

$$X(t) = I_t \tau_g \alpha_w A_{w,eff} + h_1 A_w \left[\frac{I_t \alpha_g + U_g T_{go,f}}{h_1 + U_g}\right] \quad \text{(B5)}$$

$$Y(t) = \tau_g \tau_w \alpha_p I_{pf} + U_b A_p T_a \quad \text{(B6)}$$